




A Statistical Model for Frequency of Coastal Flooding in Honolulu, Hawaii, During the 21st Century

Philip R. Thompson¹ , Matthew J. Widlansky², Mark A. Merrifield³ , Janet M. Becker³ , and John J. Marra⁴

¹Department of Oceanography, University of Hawai'i at Mānoa, Honolulu, HI, USA, ²Joint Institute for Marine and Atmospheric Research, University of Hawai'i at Mānoa, Honolulu, HI, USA, ³Scripps Institution of Oceanography, University of California, San Diego, San Diego, CA, USA, ⁴NOAA/NESDIS/National Centers for Environmental Information, Inouye Regional Center, Honolulu, HI, USA

Key Points:

- The highest sea level events in Honolulu tend to cluster together in time
- Decadal modulations of tidal amplitude temporarily reduce or enhance impacts of sea level rise
- Transitions from occasional to chronic threshold exceedance can occur in less than a decade

Supporting Information:

- Supporting Information S1

Correspondence to:

P. R. Thompson,
philiprt@hawaii.edu

Citation:

Thompson, P. R., Widlansky, M. J., Merrifield, M. A., Becker, J. M., & Marra, J. J. (2019). A statistical model for frequency of coastal flooding in Honolulu, Hawaii, during the 21st century. *Journal of Geophysical Research: Oceans*, 124, 2787–2802. <https://doi.org/10.1029/2018JC014741>

Received 7 NOV 2018

Accepted 18 MAR 2019

Accepted article online 20 MAR 2019

Published online 24 APR 2019

Abstract The state of Hawaii and city of Honolulu experienced an unprecedented number of minor flooding episodes during 2017 due to the combination of seasonal high tides and record-high mean sea levels. To quantify the impact of sea level rise on the tendency for flooding events to cluster in future years, we developed a hierarchical statistical model describing the number of days per year for which sea level exceeds a prescribed threshold in Honolulu as a function of annual mean sea level and the amplitude of the highest tides. Based on this model, we generate probabilistic projections of exceedance days per year for the 21st century, which show pronounced inflections in the frequency of exceedance days due to the interaction between sea level rise and long-period (18.6 year) modulation of tidal amplitude. Analysis of the projections demonstrates how planning for the “typical” future year can substantially underestimate flooding impacts during inevitable severe years that experience many more exceedance days than expected in a probabilistic sense. The projections also show the potential for rapid, subdecadal transitions from occasional to chronic threshold exceedance during the second half of the century, suggesting that implementation of adaptation and mitigation strategies may need to begin prior to the emergence of occasional minor impacts in affected areas.

1. Introduction

The state of Hawaii and the city of Honolulu face considerable challenges from sea level rise (SLR) due to the concentration of residents, infrastructure, high-value assets, and economic activity in the coastal zone (Hawai'i Climate Change Mitigation and Adaptation Commission, 2017). Despite these vulnerabilities, most of Hawaii has not yet experienced the routine, disruptive flooding that affects many coastal urban areas on the U.S. Atlantic Coast, such as the cities of Miami (Wdowinski et al., 2016), Norfolk (Hall et al., 2016; Sweet et al., 2014), and Boston (Ray & Foster, 2016). During 2017, however, the city of Honolulu and locations around the state of Hawaii experienced an unprecedented number of high-water episodes (Yoon et al., 2018), which included the highest hourly water level recorded by the tide gauge in Honolulu Harbor (1905 to present, Figure 1a). These events resulted in repeated overwash of famed Waikiki Beach and minor flooding of inland roads and parking lots, generating significant media attention and prompting concern about the impending impacts of SLR across the state (e.g., LaFrance, 2017).

The greatest flooding impacts experienced in Honolulu during 2017 occurred when sea levels reached approximately 35 cm above mean higher high water (MHHW), which is a vertical datum defined as the average of daily maximum water levels during the U.S. National Tidal Datum Epoch (NTDE, 1983–2001). The 35-cm threshold was qualitatively established by matching time stamps of photographs from a citizen science project documenting flooding impacts (University of Hawai'i Sea Grant College Program, 2016) to water levels recorded by the tide gauge in Honolulu Harbor. Since the gauge was established in 1905, the 35-cm threshold has been exceeded for at least 1 hr on 37 distinct days (referred to herein as *exceedance days*). Fifteen (or 40%) of these days occurred during a single 5-month period from April to August 2017.

Tallying the exceedance days in calendar years demonstrates the anomalous nature of 2017 compared to previous years, as no other year experienced more than four exceedance days above the 35-cm threshold (Figure 1b). The effect of ongoing SLR manifests in the absence of exceedances prior to the 1960s, but

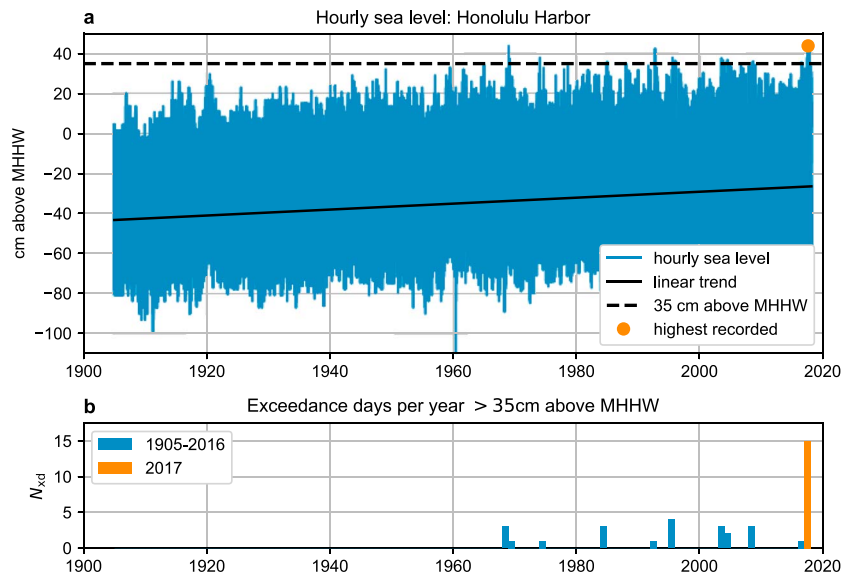


Figure 1. (a) Hourly sea level recorded by the Honolulu Harbor tide gauge (1905–2017, blue), the highest observed hourly water level (orange), and the 35 cm above mean higher high water (MHHW) minor threshold (black dashed). (b) Number of exceedance days per year (N_{xd}) above the 35-cm threshold.

SLR is not the only contributing factor, given the lack of monotonicity in the counts. The anomalous number of events during summer 2017 resulted from the superposition of multiple processes in addition to SLR (Yoon et al., 2018): the effect of decadal climate fluctuations on sea level in the Pacific (Firing et al., 2004), large-scale (>500-km zonal width) dynamic height anomalies related to oceanic planetary waves and heat flux variability at the air-sea boundary, mesoscale oceanic eddies (Chavanne et al., 2002; Firing & Merrifield, 2004), and seasonally enhanced tidal amplitudes (high tides were 5–15 cm above MHHW on exceedance days during 2017). All of these phenomena result in sea level variability with different intrinsic timescales that can—on occasion—constructively interfere to produce a cluster of high-water events (Firing & Merrifield, 2004).

A variety of methodologies exist to quantify, project, and evaluate uncertainty in the effect of mean SLR on the average return periods of the most extreme sea levels (e.g., Buchanan et al., 2017; Tebaldi et al., 2012; Wahl et al., 2017). These types of analyses are necessary and valuable, but they are not well suited for capturing the tendency for less extreme events (i.e., average return periods <1 year) to cluster together in time nor are they adept at addressing the transition of threshold exceedances from rare to routine. The topic of recurrent minor flooding has received considerable attention, because the frequency of such events is increasing in many areas (Sweet et al., 2014), and the cumulative impact of frequent minor events can exceed that of rare extremes (Moftakhari et al., 2017). The potential for cumulative impact over many minor events is particularly important for Honolulu, because despite the geographical risk for damaging surge from tropical storms, the harbor tide gauge has not recorded an hourly nontidal surge >60 cm since the record began in 1905. Projections of future minor flooding frequency show substantial increases in the average number of threshold exceedances per year in coming decades (e.g., Dahl et al., 2017; Sweet et al., 2018). However, low-frequency modulations in tidal amplitude will cause tidal flooding events to become more likely during some periods than others (e.g., Ray & Foster, 2016), and interannual to decadal variations in mean sea level (e.g., Widlansky et al., 2015) as well as secular SLR can lead to variations in the probability of minor flooding events (e.g., Vandenberg-Rodes et al., 2016). Due to the combination of long-term trends and year-to-year variability, the initial impacts of SLR will tend to occur as intermittent periods of frequent events interspersed among years with few exceedances.

Motivated by these concepts and the unprecedented number of minor flooding events in Honolulu during summer 2017, we developed a methodology for quantifying—in a probabilistic sense—when and how often prescribed impact thresholds will be exceeded by sea levels during the 21st century. We demonstrate the utility of this methodology for identifying planning horizons and for quantifying the timing and rate at which

threshold exceedances transition from occasional to chronic. The methodology is designed to be general, such that similar analyses can be conducted for any location and threshold.

2. Data

2.1. Tide Gauge Record From Honolulu Harbor

The tide gauge sea level record from Honolulu Harbor ($21^{\circ}18.4'N$, $157^{\circ}52.0'W$) began in January 1905. Datum-controlled hourly tide gauge data from Honolulu Harbor were obtained from the University of Hawai'i Sea Level Center Fast Delivery database (<http://uhslc.soest.hawaii.edu:80/opendap/fast/hourly/h057.nc>), which extends the Research Quality record (accessed July 2018; Caldwell et al., 2010) from the end of 2016 to present.

2.1.1. Tidal Analysis

We generated deterministic tidal predictions based on harmonic analysis of the hourly water levels measured by the Honolulu Harbor tide gauge. Observations during the 19-year U.S. NTDE (1983–2001) were used to cover a full lunar nodal cycle. Tidal harmonics and the associated predicted future water levels were calculated using the Unified Tidal Analysis and Prediction “UTide” procedure (Codiga, 2011). The generated tidal predictions are based on 68 harmonic constituents, which include the annual, semiannual, and nodal cycles. The latter relates to the 18.6-year wobble of the Moons orbit around the Earth. Harmonics were calculated from the NTDE as a whole, rather than performing the calculations year by year. While there are typically some variations between different tidal prediction products, such as from the National Oceanic and Atmospheric Administration (NOAA) Center for Operational Oceanographic Products and Services, we found our procedure to describe well the observed tidal oscillations at Honolulu and for other locations with sufficiently long records (Widlansky et al., 2017).

2.1.2. Separation of Tidal and Nontidal Variability

The methodology developed here relies on the joint probability of tidal, dynamical, and secular contributions to sea level variability. Achieving these joint probabilities requires clean separation of the tidal and nontidal variability in the observations. To evaluate the effectiveness of the tidal analysis (section 2.1.1), we subtracted the predicted tide from the observations and apply a convolution high-pass filter to the residuals passing >80% of the variance at 24 hr and >99% of the variance at 21 hr. The subdaily residuals reveal a marked difference in the effectiveness of the tidal prediction between early and late portions of the record (Figure 2a). Specifically, there is a reduction in the 99th percentile of the subdaily residuals from 9.3 cm during 1905–1947 to 5.2 cm during 1948–2017.

The abrupt reduction in subdaily residual variance corresponds to a change in the Hawaii time zone from GMT-10.5 hr to GMT-10 hr on 13 June 1947 (see metadata for the Honolulu Harbor tide gauge record here: <https://uhslc.soest.hawaii.edu/rqds/pacific/doc/qa057b.dmt>). The time zone change causes the tidal prediction generated from data during the NTDE to be off by half an hour prior to the time zone change. The digitized hourly data from Honolulu Harbor represent spot samples on the hour, so it is not appropriate to interpolate the pre-1947 observations to the current time zone, as this would tend to mute the amplitude of the most extreme levels. Instead, we interpolated the tidal prediction to the correct times prior to the time zone change. Subtracting the time-zone-adjusted tidal prediction from the observations deflates the subdaily residual variance in the early part of the record, but the 99th percentile remains more than 50% greater in the early period (Figure 2b). The remaining difference can be attributed to additional timing issues that become apparent after adjusting the tidal prediction for the time zone change (Figures 2c and 2d). The combined effect of the time zone offset and additional inconsistencies in timing may at least partially account for the decreasing trend in number of extreme sea levels unrelated to mean sea level variability found in the Honolulu record (Marcos et al., 2015).

Correcting the remaining timing issues is beyond the scope of this work, but they represent nonphysical contamination of the distribution of nontidal sea levels. These issues have the potential to adversely affect our estimates of the contribution from nontidal variability to the frequency of threshold exceedances. Thus, in the analysis that follows, we restricted usage of the 113 years of tide gauge data from Honolulu Harbor to the 90 years, which are 95% complete and for which the 99th percentile of subdaily tidal residuals is <7 cm. The former criterion excludes six years: 1921, 1942, 1973, 1976, 1977, and 1992. The latter criterion excludes nine additional years: 1908–1911, 1920, 1923, 1927, 1928, and 1945, all of which were verified to exhibit subdaily residual variability similar to that shown in Figures 2c and 2d.

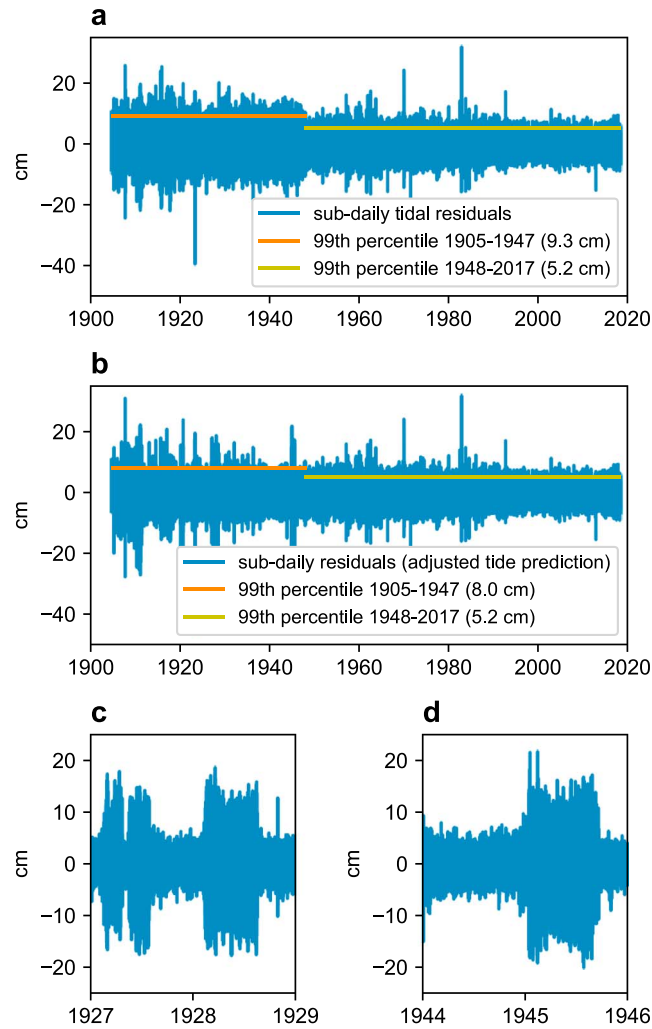


Figure 2. (a) Subdaily tidal residuals from Honolulu Harbor (blue) and 99th percentiles of the subdaily residuals for 1905–1947 and 1948–2017 (orange and yellow, respectively). (b) Same as (a) but using an adjusted tidal prediction during 1905–1947, accounting for a half hour offset in the time zone prior to 1948. (c) Zoomed section of (b) showing an example of timing issues remaining in the early part of the record after adjusting the tidal prediction. (d) Same as (c).

3. Methods

The following sections outline a framework for making probabilistic projections of threshold exceedance days during the 21st century. We began by hypothesizing that the probability distribution governing the number of exceedance days during a given year can be described as a function of two quantities: annual mean sea level and the amplitude of the largest astronomical tides during the year. Subannual mean sea level variations dictate where the number of exceedance days falls within that distribution. Specifically, we represented the combined effect of these two factors as a single parameter, η_{99} , defined as the sum of two terms:

$$\eta_{99} \equiv \bar{\eta}_{\text{res}} + \zeta_{99}, \quad (1)$$

where $\bar{\eta}_{\text{res}}$ is the annual mean of the nontidal residual variability and ζ_{99} is the annual 99th percentile of predicted astronomical tidal heights relative to the current tidal datum. The analysis that follows is not particularly sensitive to the choice of percentile in the latter, as long as the choice captures long-period modulations of tidal amplitude (e.g., the 18.6-year nodal cycle). In effect, η_{99} represents an update to the predicted height of the highest tides based on the amount of background mean sea level elevation. Importantly for the present application, it is possible to make informed 21st century projections for each term on

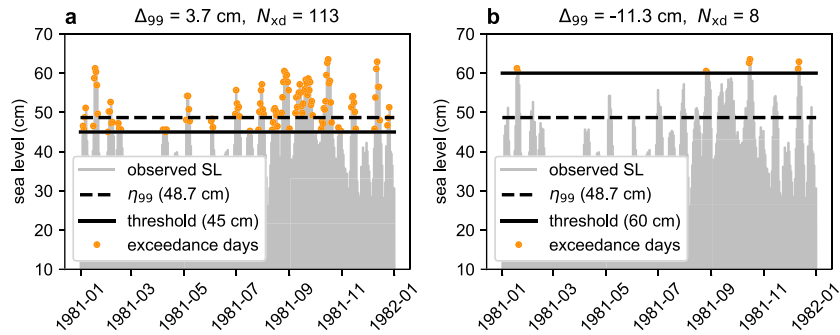


Figure 3. Examples of iterations in the threshold experiment for a randomly selected year (1981) when Δ_{99} is (a) positive and (b) negative. Sea levels (SLs) are extracted from the detrended and demeaned time series of Honolulu sea level, and hence, values represent height relative to the trend line.

the right-hand side of equation (1). Astronomical tides (and hence ζ_{99}) are deterministic and can be predicted with high accuracy many decades in advance (section 2.1.1). While it is not possible to make exact predictions of annual mean sea level variability (i.e., $\bar{\eta}_{\text{res}}$) due to year-to-year stochasticity associated with coupled atmosphere-ocean dynamics, the secular portion of annual mean sea level change related to a warming Earth can be projected (with some uncertainty) into the future using climate models forced by various scenarios of increasing greenhouse gas emissions (section 3.3.1).

3.1. Threshold Experiment

To investigate how the distribution of exceedance days varies with η_{99} , we performed a simple threshold experiment. We began with the detrended and demeaned hourly sea level record from Honolulu and counted the number of exceedance days in each year above a series of thresholds increasing in steps of 1 cm (with years limited as discussed in section 2.1.2). We also calculated the η_{99} corresponding to each count. Two examples from a randomly chosen year (Figure 3) demonstrate how the number of exceedance days decreases as threshold height increases relative to the observed sea level variability. More importantly, we note that a greater number of exceedance days occur when η_{99} is near or above the threshold (Figure 3a) compared to when η_{99} is substantially below the threshold (Figure 3b). This is true regardless of the absolute value of either the threshold height or η_{99} . In other words, if mean sea level rises 50 cm, but we also raise the threshold by 50 cm, we expect the same probability of exceedance. Thus, the relevant quantity for projecting exceedance days above a given threshold is the difference between η_{99} and the threshold, denoted hereafter as Δ_{99} and defined

$$\Delta_{99} \equiv \eta_{99} - \text{threshold}, \quad (2)$$

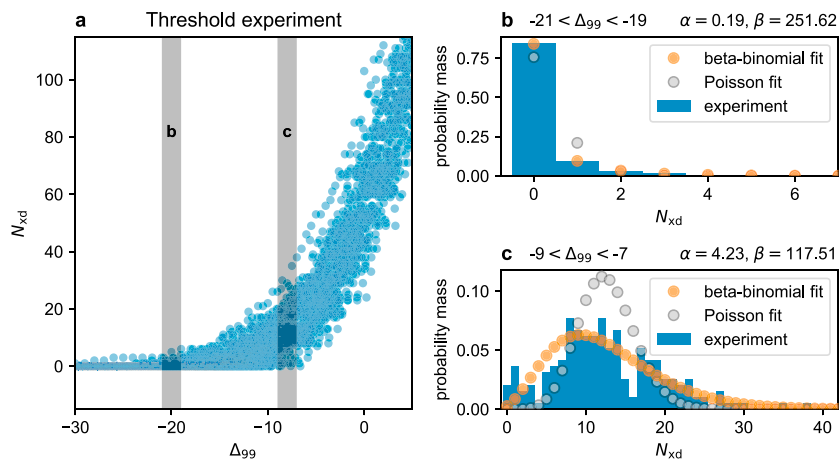


Figure 4. (a) Sample counts of exceedance days per year (N_{xd}) from the threshold experiment Δ_{99} (i.e., the difference between η_{99} and height of the threshold). (b and c) Histograms of counts in selected 2-cm intervals of the Δ_{99} space (blue) and maximum likelihood fits of Poisson (gray) and beta-binomial (orange) probability mass distributions to the histograms. The 2-cm intervals represented in (b) and (c) are highlighted by vertical bars in (a).

such that $\Delta_{99} < 0$ when η_{99} is below the threshold (as in Figure 3b).

A scatter plot of the annual counts of exceedance days (denoted hereafter as N_{xd}) from the experiment versus Δ_{99} demonstrates how the number and distribution of exceedance days changes as η_{99} approaches and exceeds a given threshold (Figure 4a). Very few exceedance days occur when $\Delta_{99} < -20$ cm, because few subannual, nontidal anomalies in Honolulu have sufficient amplitude to push total sea level over the threshold. As η_{99} increases toward the threshold (i.e., $\Delta_{99} \rightarrow 0$ cm) along the horizontal axis, the number of exceedance days increases as smaller subannual, nontidal anomalies become capable of elevating sea level above the threshold.

3.2. Modeling the Relationship Between Δ_{99} and Threshold Exceedance Days

Histograms of N_{xd} from the experiment in 2-cm bands of Δ_{99} show how the shape of the distribution changes with Δ_{99} . At about -20 cm (Figure 4b), the histogram is narrow and highly skewed with the histogram becoming broader and more symmetric as Δ_{99} increases toward 0 (Figure 4c). We looked for probability mass functions to describe the evolution of the distribution as a function of Δ_{99} , which can then be used to generate probabilistic projections of exceedance days from deterministic tidal predictions and probabilistic projections of annual mean sea level.

Counts of sea level exceedances per year above a threshold are often assumed to follow a Poisson distribution (e.g., Cid et al., 2016; Rasmussen et al., 2018). Maximum likelihood estimates of the Poisson probability mass function that best describe the histograms from the Honolulu threshold experiment show some similarity with the histogram at low values of Δ_{99} (Figure 4b). Even a modest increase in Δ_{99} , however, shows substantial overdispersion in the histogram relative to the Poisson shape (Figure 4c). The poor fit is due to violating key assumptions of Poisson distributed counts, including that the probability of an event is constant in time and that the number of binomial trials (in this case $N = 365$ days) is sufficiently larger than the number of binomial successes (i.e., threshold exceedances). Alternatively, the beta-binomial distribution (Skellam, 1948) offers a more general representation of binomially distributed counts that is useful when data are overdispersed relative to more commonly used models (Kim & Lee, 2017). Maximum likelihood estimates of beta-binomial distributions that best fit the histograms from the threshold experiment produce distribution shapes more likely to represent the true underlying distributions compared to the Poisson fits (Figures 4b and 4c).

We developed a hierarchical model based on the beta-binomial distribution for the number of exceedance days in a year as a function of Δ_{99} (Text S1 in the supporting information). The model can be summarized as follows:

$$\begin{aligned} \mathbf{X} | \Delta_{99}, \xi, \omega, \nu &\sim \text{BetaBinomial}(N, \boldsymbol{\mu}, \boldsymbol{\sigma}^2), \\ \boldsymbol{\mu} &= S(\Delta_{99}; \xi, \omega), \\ \boldsymbol{\sigma}^2 &= \nu \boldsymbol{\mu}(1 - \boldsymbol{\mu}), \end{aligned} \quad (3)$$

where \mathbf{X} and Δ_{99} are vectors containing the results of the threshold experiment (i.e., Figure 4a) and $\boldsymbol{\mu}$ and $\boldsymbol{\sigma}^2$ are vectors of parameters that determine the shape of the beta-binomial distribution at each value in Δ_{99} . The vectors of parameters $\boldsymbol{\mu}$ and $\boldsymbol{\sigma}^2$ are proportional to the mean and variance, respectively, of the beta-binomial distribution for each element in Δ_{99} . The function S in the second equation of (3) represents the normal cumulative distribution function (Text S1), which is used to model the vector $\boldsymbol{\mu}$ as a function of the elements in Δ_{99} and is defined by scalar location and scale parameters, ξ and ω . The elements in $\boldsymbol{\sigma}^2$ are related to the elements in $\boldsymbol{\mu}$ by the third relation in (3), which depends on the scalar parameter $\nu \in (0, 1)$ and is derived from the definition of the beta-binomial distribution (Text S1).

We used Bayesian inference implemented via Markov Chain Monte Carlo to estimate the free parameters of the model, $\{\xi, \omega, \nu\}$, as random variables with probability distributions conditioned on the results of the threshold experiment (Text S2). The medians and approximate 95% credible intervals for the parameters are as follows:

$$\begin{aligned} \xi &= 10.2 \pm 0.4, \\ \omega &= 10.1 \pm 0.3, \\ \nu &= (7.5 \pm 2.0) \times 10^{-3}. \end{aligned} \quad (4)$$

The credible intervals are not strictly symmetric, but they are approximately symmetric. For simplicity, the credible intervals above are given as plus-minus the credible interval bound with the largest absolute difference from the median.

The model in (3) and parameter posteriors in (4) give posterior values of μ and σ^2 as functions of Δ_{99} that are consistent with counts from the threshold experiment (Figure S1). Thus, given a threshold of interest and a projected value of η_{99} for a future year, we can calculate Δ_{99} and use the posterior parameter distributions above to calculate the probability of a given number of exceedance days above a prescribed threshold. This probability incorporates stochastic variability in the phasing and amplitude of processes that lead to threshold exceedances (i.e., the shape of the distribution), as well as uncertainty in the model that best represents the stochastic variability (i.e., uncertainty in the parameters that determine the shape of the distribution).

3.3. The 21st Century Projections of η_{99}

Projecting η_{99} in Honolulu during the 21st century requires three components. The first is secular local mean sea level (LMSL) rise related to forced climate variability and a warming Earth. The second is annual LMSL variability related to atmosphere-ocean dynamics and internal climate variability. The third is the annual 99th percentile of astronomical tidal height relative to current tidal datums. We estimated each of these components independently, and the three were summed to create projections of η_{99} . Details of the approach for each component follow.

3.3.1. Secular LMSL Rise Projections

Global mean SLR projections from the Intergovernmental Panel on Climate Change (IPCC) AR5 report (Church et al., 2013) provide a reasonable starting point for estimating future mean sea level in Honolulu, but it is important to consider that local sea level change can substantially differ from global average rise. We utilized two variants of LMSL projections that include location-specific factors such as glacial isostatic adjustment and regional patterns of sea level change due to the impact of ice melt on Earth's gravitational and rotational fields. The projections were placed into the reference frame of the tide gauge data by setting the initial value of the projections in the year 2000 to the mean nontidal sea level from the tide gauge observations over the 19-year period 1991–2009. The nontidal sea level variability has zero mean over the NTDE, so adding projected mean sea level to a predicted astronomical tidal height relative to MHHW defined over the NTDE gives units of sea level relative to MHHW.

The first variant of LMSL projection for Honolulu is a probabilistic projection from Kopp et al. (2014) based on the IPCC AR5 RCP8.5 emissions scenario (hereafter Kopp14). The projection is based on the Coupled Model Intercomparison Project phase 5 (Caldwell et al., 2010), expert elicitation, and estimates of nonclimatic background processes obtained from tide gauge observations. We obtained 10^4 realizations of 21st century Honolulu LMSL from the probabilistic projection using the code repository supplement to Kopp14 (<https://github.com/bobkopp/LocalizeSL>). Each realization includes variance associated with ocean dynamics from Coupled Model Intercomparison Project phase 5, but we estimated this component of the variability from the observations instead (section 3.3.2), because the decadal resolution of the publicly available Kopp14 projections do not capture year-to-year variability essential to this analysis. Thus, we modified the code to include variability in global mean steric height only instead of local steric height (i.e., CMPI5 variable *zostoga* instead of variable *zos*). Lastly, we interpolated the one-value-per-decade resolution of each realization to annual resolution via cubic spline. The Kopp14 probabilistic projections of LMSL give fairly tight likely and very likely ranges but with long tails representing possible yet low probability extreme cases (Figure 5a).

The second variant is the U.S. NOAA SLR scenarios (Sweet et al., 2017) obtained from the NOAA Center for Operational Oceanographic Products and Services (<https://tidesandcurrents.noaa.gov/publications/techrpt083.csv>). These scenarios aim to alleviate difficulty in applying projections with broad uncertainty ranges by providing discrete projections with guidance on how to choose a projection based on application and risk tolerance. The six discrete projections of Honolulu LMSL (Figure 5b) correspond to scenarios where global mean SLR by 0.5, 1.0, 1.5, 2.0, 2.5, and 3.0 m by the year 2100. The low and extreme scenarios represent the scientifically plausible upper and lower bounds on Honolulu SLR during the 21st century. We utilized the three intermediate scenarios and interpolated the one-value-per-decade resolution of each scenario to annual resolution via cubic spline. For context, the likely range of the Kopp14 projection (Figure 5a) falls between the discrete “intermediate-low” and “intermediate” NOAA scenarios (Figure 5b).

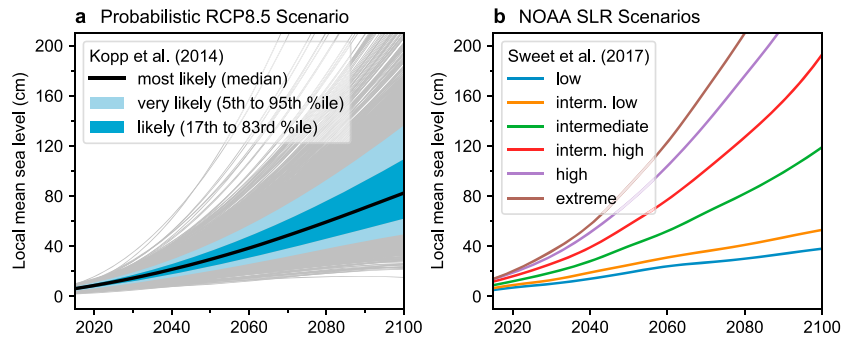


Figure 5. Projections of 21st century local mean sea level for Honolulu. (a) A probabilistic projection for the Intergovernmental Panel on Climate Change AR5 Representative Concentration Pathway (RCP8.5) scenario (Kopp et al., 2014). (b) National Oceanic and Atmospheric Administration (NOAA) sea level rise (SLR) scenarios (Sweet et al., 2017).

3.3.2. Simulating Nonsecular Annual LMSL Variability

We modeled stochastic, nonsecular annual LMSL variability as a function of year, $a(y)$, with a zero-mean Gaussian process,

$$a(y) \sim \text{GP}(0, K(y, y')) + \epsilon, \quad (5)$$

where K is a covariance function determining serial correlation in the time series and $\epsilon \sim \mathcal{N}(0, \Sigma)$ is normally distributed noise with zero mean and variance Σ . We chose a rational quadratic covariance function,

$$K(y, y') = A^2 \left(1 + \frac{(y - y')^2}{2bl^2} \right)^{-b}, \quad (6)$$

where A^2 is the variance of the process, l is a fundamental lengthscale, and b determines the relative weighting of long- and short-scale variations in the process. We searched via numerical optimization for the most likely values of the parameters given the detrended observed annual LMSL variability from the Honolulu tide gauge (Figure 6a). The optimized parameter values rounded to the nearest tenth are $A^2 = 5.4$, $l = 10.3$, $b = 1.0$, and $\Sigma = 2.4$. Random samples from the Gaussian process with these parameters provide reasonable realizations of stochastic annual LMSL variability in Honolulu during the 21st century (Figures 6b–6d). We generated 10^4 samples from the Gaussian process to use in the probabilistic projections of N_{xd} . All years

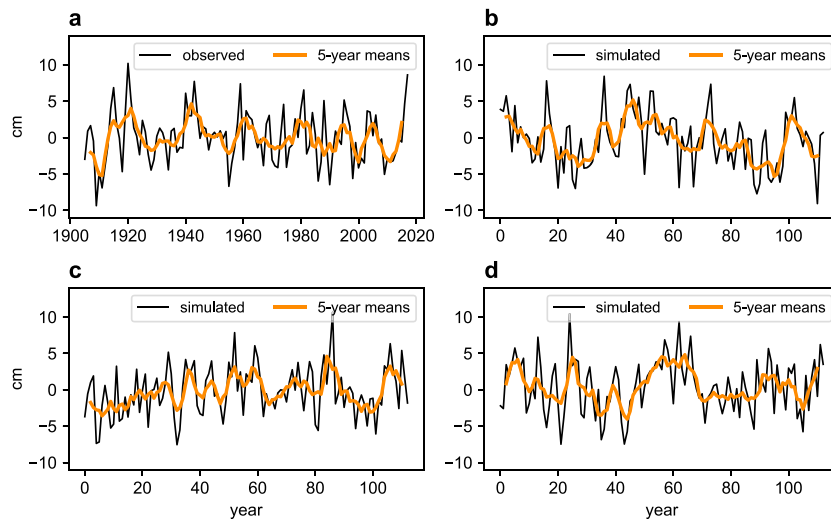


Figure 6. (a) Observed annual local mean sea level variability from the Honolulu tide gauge record (black) and 5-year running means (orange). (b–d) Random samples from the optimized Gaussian process (black) and 5-year running means (orange).

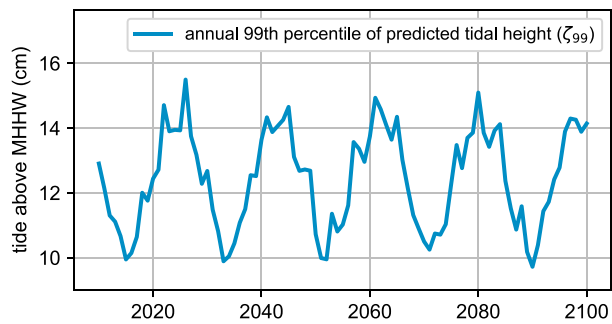


Figure 7. The 99th percentile of the predicted astronomical tide (ζ_{99}) for Honolulu in each year during the 21st century.

in the Honolulu tide gauge record (1905–2017) were used in this step, as the annual mean sea level is not affected by the subdaily timing issues that necessitated exclusion of some years in the threshold experiment. Finally, we note that a limitation of this approach is that it does not account for the possibility that the statistics of interannual and longer LMSL variability may not be stationary during the 21st century. We expect the effect of nonstationarity to be small, however, and including this potential is left to be addressed in future work.

3.3.3. The 99th Percentile of Astronomical Tides

Tidal constituents estimated from harmonic analysis of the Honolulu tide gauge data (section 2.1.1) were used to predict astronomical tides relative to the current MHHW datum for the 21st century. We used the 99th percentile of the predicted astronomical tide in each year (ζ_{99} , Figure 7) as a proxy for modulations in tidal amplitude in the projections of η_{99} .

The dominant periodicity of low-frequency (i.e., longer than annual) tidal

modulation in Honolulu is the 18.6-year nodal cycle (e.g., Haigh et al., 2011), which leads to peak-to-trough variations in ζ_{99} of approximately 5 cm. We note that SLR can also induce changes in tidal amplitude, especially in seas situated along continental shelves, but this effect is generally small for open ocean island locations like Hawaii (Pickering et al., 2017). The effect is not of leading order in Honolulu and is not considered here.

3.4. Projections of Exceedance Days per Year (N_{xd})

To produce probabilistic 21st century projections of N_{xd} above a given threshold, we performed the following procedure:

1. Subtract the threshold height from the 10^4 projections of η_{99} to calculate Δ_{99} (as in the threshold experiment, section 3.1).
2. For each year in the 21st century, assign each of the 10^4 values of Δ_{99} to one of the 10^4 draws from the posterior distributions of the model parameters in (4).
3. Draw random values from beta-binomial distributions with shapes determined by the model in (3) and the combinations of Δ_{99} and model parameters to produce 10^4 time series representing possible realizations of 21st century exceedance days per year.

4. Results

The results that follow pertain to two passive flooding thresholds. The first is 35 cm above MHHW, which is an approximate threshold for isolated minor flooding impacts in Honolulu exceeded on fifteen days during 2017 (Figure 1). The second is 90 cm above MHHW representing a scenario in which passive flooding occurs across vast areas of coastal Honolulu, including substantial portions of the state's economic hub, Waikiki (Figure 8). To demonstrate the extent of areas impacted by sea levels above the 90-cm threshold in Honolulu, we used a digital elevation map based on lidar topographic data with 1-m resolution from the U.S. Army



Basemap: CartoDB Positron (<https://cartodb-basemaps-a.global.ssl.fastly.net>) made using open data published by OpenStreetMap and NaturalEarth.

Figure 8. Flooding depth in the Waikiki region of urban Honolulu when sea level reaches 90 cm above mean higher high water. The map includes the effect of groundwater inundation in areas not hydrologically connected to the ocean (Habel et al., 2017). Warm colors denote areas that are dry when sea levels are below the current mean higher high water datum.

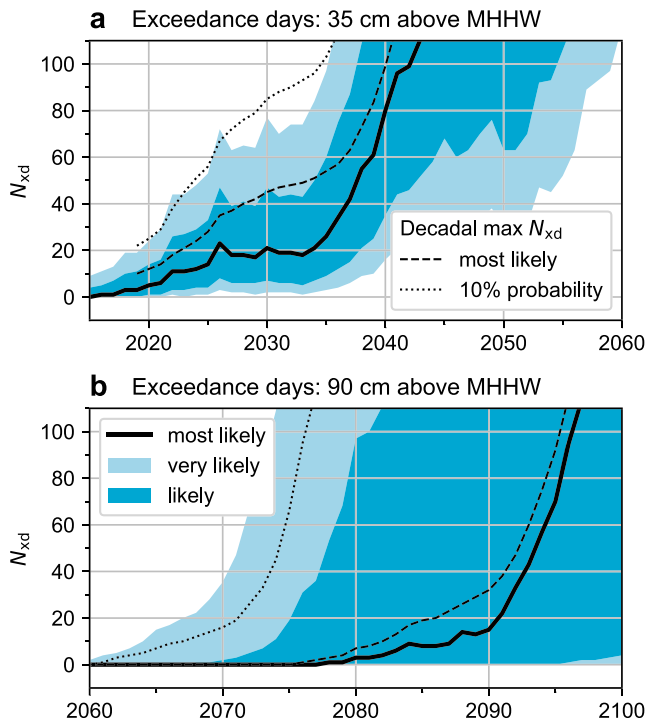


Figure 9. The 21st century projections of exceedance days per year based on the Representative Concentration Pathway (RCP8.5) scenario from Kopp et al. (2014) for thresholds (a) 35 cm above mean higher high water (MHHW) and (b) 90 cm above MHHW. Black solid lines represent the most likely (median) annual counts of exceedance days; shading represents *likely* (17–83%) and *very likely* (5–95%) probability intervals. Dashed and dotted lines represent the most likely and 10% probability values for the maximum N_{xd} during the decade preceding each year. The legend is split between panels, but each legend frame applies to both (a) and (b).

Corps of Engineers (OCM Partners, 2018) modified such that the elevations are relative to the height of the groundwater table (Habel et al., 2017). Thus, using this digital elevation map to assess which grid cells are flooded under a given sea level includes the potential for groundwater to flood areas not hydrologically connected to the ocean (Habel et al., 2017). These thresholds are subjectively chosen, but the framework outlined here can be used to create projections of exceedance days above any threshold deemed relevant for developing adaptation and mitigation strategies. We present the results of the probabilistic projections as percentiles of counts from the procedure in section 3.4, which can be interpreted as probability intervals for the number of exceedance days in each 21st century year. *Likely* and *very likely* ranges correspond to the 17–83% and 5–95% likelihood intervals, respectively, as defined in the IPCC AR5 report (Cubasch et al., 2013).

4.1. Projections of Exceedance Days

Likely ranges for exceedance days above the 35-cm threshold for Kopp14 (Figure 9a) increase rapidly over the next two decades from [1, 14] in 2020 to [7, 47] in 2030, and to [36, 149] in 2040. Aside from the general trajectory toward greater numbers, the salient feature of this projection is the flattening of the curve from the mid-2020s to the mid-2030s, followed by a rapid increase in the expected number and likely ranges of exceedance days. This inflection results from the interaction between increasing rates of LMSL change and long-period variations in ζ_{99} related to the 18.6-year nodal cycle in tidal amplitude (Figure 7). The amplitude of the highest tides of the year decreases by roughly 5 cm from the mid-2020s to the mid-2030s. The *likely* range of LMSL rise over the same period from the Kopp14 projection is approximately [5, 8] cm (Figure 5a). Thus, the effect of LMSL increase on the number of exceedance days per year is largely countered by decreasing tidal amplitude during this time. The subsequent rapid increase occurs as increasing tidal amplitude syncs with continued increase in the rate of background LMSL change. Note that the shorter-term fluctuations apparent in the expected and *likely* ranges are

not indicative of noise due to under sampling the distribution. Rather, these fluctuations are the result of predicted year-to-year fluctuations in tidal amplitude.

The *likely* ranges of N_{xd} for the 35-cm threshold under the intermediate and intermediate-low NOAA scenarios (Figure 10a) bracket the likely ranges for the Kopp14 projection. *Likely* ranges for the intermediate-low scenario increase from [1, 13] in 2020 to [5, 30] in 2030, and to [28, 86] in 2040. *Likely* ranges for the intermediate scenario increase from [3, 23] in 2020 to [22, 75] in 2030, and to [102, 207] in 2040. The intermediate and intermediate-low scenarios show an inflection in the number of exceedance days around the mid-2030s similar to the inflection for the Kopp14 scenario. For the intermediate-high scenario, the higher rates of SLR overwhelm the influence of long-period tidal modulation, and the inflection does not manifest.

The probability of exceedances above the 90-cm threshold is vanishingly small for the Kopp14 and NOAA LMSL rise scenarios until the second half of the 21st century. Appreciable probabilities emerge for the Kopp14 projection during the 2060s (Figure 9b), but the number of exceedance days for a given year is highly uncertain due to growing uncertainties in projected LMSL rise by the late 21st century (Figure 5a). The most likely number of exceedance days above 90 cm in 2080 is three, but the likely range includes the possibility of up to 97. In contrast, the discrete NOAA scenarios—which exclude late century LMSL uncertainty by design—show narrow *likely* ranges in comparison and rapid transitions over ≈ 15 years from few (<5) to many (>100) expected exceedance days per year. The transition occurs in the 2050s–2060s for the intermediate-high scenario and during the 2070s–2080s for the intermediate scenario. The probability of exceedance days remains approximately zero for the intermediate-low scenario throughout the 21st century.

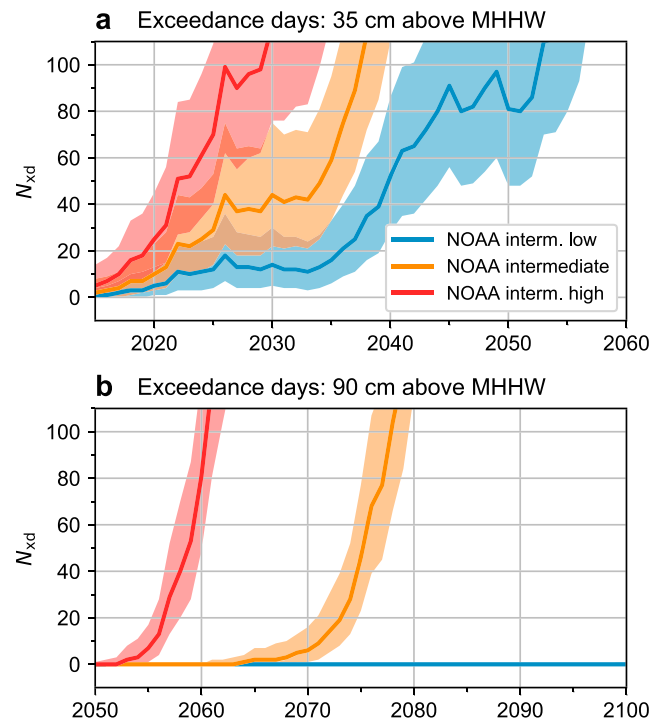


Figure 10. The 21st century projections of exceedance days per year based on the discrete National Oceanic and Atmospheric Administration (NOAA) scenarios (Sweet et al., 2017) for thresholds (a) 35 cm above mean higher high water (MHHW) and (b) 90 cm above MHHW. Dark lines represent the most likely (median) annual counts of exceedance days; shading represents likely (17–83%) probability intervals.

4.2. Interpretation of the Projections

The probabilistic projections of exceedance days (Figures 9 and 10) are difficult to apply in definitive decision making, because for any given year and scenario, the width of the likely range is generally the same order of magnitude as the expected value. However, the probabilistic projections developed here can be reframed to extract features of the projections relevant for decision making. Rather than focusing on the number of exceedance days to expect in a specific year, we offer the following perspectives. While not comprehensive, these perspectives demonstrate the flexibility and potential utility of the probabilistic projections for planning and mitigation in Honolulu and elsewhere.

4.2.1. Inevitable Severe Years

The highest water levels in Honolulu tend to cluster together in time as demonstrated by the unprecedented number of minor flooding events during 2017. Multiple oceanographic phenomena in the region cause sea level variations with independent timescales and phasing that occasionally align to produce “bursts” of high-water events. The threshold experiment (section 3.1) highlights this tendency, especially for lower values of Δ_{99} when η_{99} is substantially below the threshold of interest. Counts of exceedance days per year for values of Δ_{99} around -20 cm produce a large number of years with zero exceedance days and a small number of higher-density years (Figure 4b). Parsing the values that make up the histogram reveals that roughly 50% of exceedance days in this range of Δ_{99} occur in about 3% of the years.

The tendency for high-water events to cluster in time has important implications for those tasked with planning for the impacts of SLR. In particular, planning for the “typical” future year can lead to substantial underestimation of event frequency during occasional—yet inevitable—severe years. Consider the projection of N_{xd} for the 35-cm threshold and Kopp14 LMSL rise scenario (Figure 9a). According to this projection, the most likely N_{xd} in 2030 is 21. It is important to note, however, that the probability ranges correspond to N_{xd} in specific years and do not adequately portray the inevitability that some years will experience numbers of exceedance days outside the likely range. To demonstrate this, we calculated the probabilities of maximum N_{xd} in the 10-year period prior to (and inclusive of) each year in the projection. In other words, for 2030, we calculate the probability of the maximum N_{xd} during 2021–2030. The 50th and 90th percentiles of this calculation for each year are shown with the projections in Figure 9a; the former corresponds to the

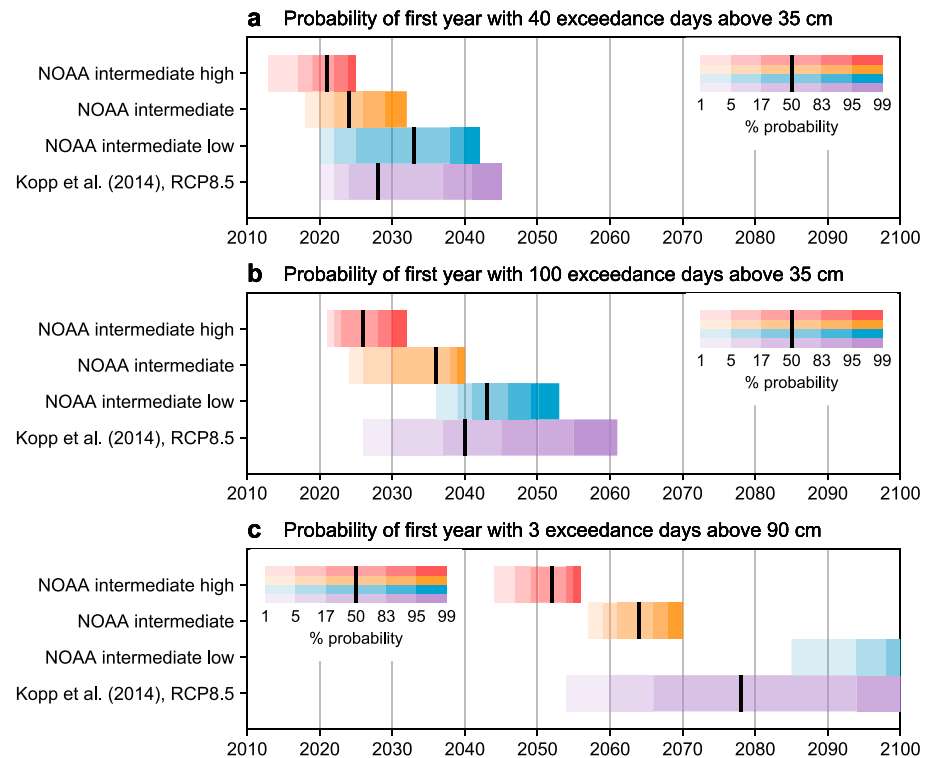


Figure 11. Probabilities of first year to experience (a) 50 exceedance days above the 35 cm above mean higher high water (MHHW) threshold, (b) 100 exceedance days above the 35 cm above MHHW threshold, and (c) 3 exceedance days above the 90 cm above MHHW threshold. Vertical black lines correspond to the most likely (or 50% probability) year. Color palettes correspond to different local mean sea level rise scenarios. NOAA = National Oceanic and Atmospheric Administration.

most likely N_{xd} during the worst year of the decade. This exercise shows that the most likely number of exceedance days during the worst year of the 2021–2030 period is about 45, or more than double the expected number for 2030 specifically. Perhaps more importantly, there is a 10% chance that at least 1 year during 2021–2030 will experience 85 or more exceedance days. Similar conclusions about the expected value of N_{xd} for an individual year versus the preceding decade can be drawn for any year in the projection. Thus, at-risk infrastructure and urban systems may need to tolerate numbers of threshold exceedances during inevitable severe years that far exceed what is “expected” for a given year in a probabilistic sense.

4.2.2. Identifying Planning Horizons

Planning horizons are an important component of adaptation and mitigation strategies. The probabilistic projections developed here allow for probabilities to be assigned to the year that first experiences some number of exceedance days above a given threshold. This type of analysis is similar to the concept of expected waiting time until a single exceedance, which has been proposed as a key risk measure when planning for climate change (Olsen et al., 1998). We focus on the specific year rather than a time interval from present to prevent the results from becoming dated as the expected waiting time decreases in the future. We demonstrate this capability for three cases (Figure 11): $N_{xd} = 50$ for the 35-cm threshold, $N_{xd} = 100$ for the 35-cm threshold, and $N_{xd} = 3$ for the 90-cm threshold. The first two cases represent degrees of recurrent minor flooding, while the latter case represents widespread disruptive flooding occurring more often than isolated extremes. For each case, we calculated the probability of the first year of occurrence for each LMSL rise scenario utilized in the projections of exceedance days.

Results of this calculation suggest there is high likelihood (>83%) across all LMSL scenarios that the city of Honolulu will experience 50 exceedance days above the 35-cm minor flooding threshold in a single year prior to the end of the 2030s (Figure 11a). The more severe NOAA intermediate and intermediate-high scenarios suggest high likelihood of occurrence by the end of the 2020s. This case represents more than triple the number of exceedance days during the record-setting summer of 2017 with high probability of occurrence in the next two decades and potentially in the next 10 years. For the second case, there is greater than

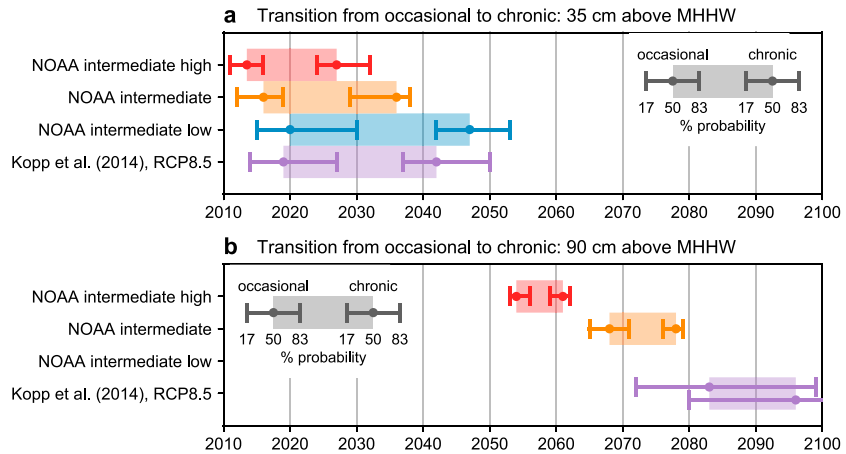


Figure 12. Span of transition from occasional to chronic numbers of exceedance days. (a) 35 cm above MHHW threshold. (b) 90 cm above mean higher high water (MHHW) threshold. The leftmost extent of each shaded bar represents the most likely year when a value of η_{99} consistent with occasional exceedance first occurs. The rightmost extent corresponds to the same quantity but for chronic exceedance. The whiskers correspond to likely ranges. NOAA = National Oceanic and Atmospheric Administration; RCP = Representative Concentration Pathway.

50% probability across all scenarios that the number of 35-cm exceedance days will exceed 100 in a single year by the early 2040s (Figure 11b). The NOAA intermediate and intermediate-high scenarios project this to occur by the mid- to late-2030s. Thus, there is significant potential for the city of Honolulu to experience impacts similar or worse than the events of 2017 on more than a quarter of the days in a single year sometime in the next two decades. Finally, for the higher 90-cm threshold, probabilities of the first year with three exceedance days vary vastly between the LMSL rise scenarios, which reflects the growth of uncertainty in LMSL projections during the second half of the 21st century (Figure 11c). The Kopp14 projection of LMSL rise implicitly includes this uncertainty, while uncertainty in LMSL manifests in the NOAA discrete scenarios as widening spread between the scenarios. Based on the Kopp14 projection, the transition from rare to occasional passive flooding at the 90-cm level will most likely occur during the last quarter of the 21st century. We note, however, that the NOAA intermediate-high scenario is within the bounds of scientifically plausible LMSL rise (Sweet et al., 2017) and the potential for transition to occasional exceedance of the 90-cm threshold is possible as early as the late 2040s.

4.2.3. Transition From Occasional to Chronic

Returning to the threshold experiment, we highlight that the scale of Δ_{99} along the horizontal axis in Figure 4a is a fraction of the expected LMSL rise during the 21st century across all scenarios (Figure 5). Thus, the transition from occasional to chronic threshold exceedances in Honolulu will occur over a period of decades. Here we used the model in equation (3) to calculate the change in η_{99} corresponding to the transition from occasional to chronic and use the LMSL projections to calculate when the transition will occur. We defined “occasional” exceedance when only 1 in 10 years experiences more than 10 exceedance days, which is roughly representative of the current situation in Honolulu relative to the 35-cm minor flooding threshold. We defined “chronic” exceedance to be when 9 in 10 years experience more than 50 exceedance days, which also corresponds to when 6 in 10 years experience more than 100 exceedance days. For Honolulu, just 15 cm separates occasional exceedance at $\eta_{99} = 13$ cm below the threshold of interest (i.e., $\Delta_{99} = -13$ cm) from chronic exceedance at $\eta_{99} = 2$ cm above the threshold of interest (i.e., $\Delta_{99} = 2$ cm). Based on the projections of η_{99} , we estimated the timing and duration of this transition for each threshold and LMSL rise scenario (Figure 12).

For the 35-cm threshold, the transition from occasional to chronic exceedance spans the present to roughly two decades in the future for the Kopp14 and NOAA intermediate LMSL rise scenarios (Figure 12a). The transition occurs slightly slower for the NOAA intermediate-low scenario and slightly faster for the NOAA intermediate-high scenario. In contrast, transitions for the 90-cm threshold occur over less than a decade (Figure 12b). The onset and completion of the transition is highly uncertain in the case of the Kopp14 scenario and 90-cm threshold, which is due to large uncertainty in the LMSL projection late in the century. There is considerably less uncertainty in the length of the transition, however, with a distribution centered

on 10 years with a likely range of [5, 14] years (not shown). In general, the length of time associated with the transition is inversely related to the rate of LMSL rise. Faster rates of LMSL change correspond to shorter transition periods.

5. Summary and Discussion

The state of Hawaii and city of Honolulu experienced an unprecedented number of minor flooding episodes during 2017 due to the combination of seasonally high tides and multiple oceanographic processes resulting in record-high mean sea levels. The events in Honolulu demonstrate the tendency of the highest water levels to cluster together in time, which implies that as sea levels continue to rise, exceedances above flooding thresholds will initially be concentrated in a small number of severe years separated by years of little to no impact. To quantify this tendency, we developed a statistical model describing the probability distribution of exceedance days per year above a prescribed threshold in Honolulu. Specifically, annual counts of exceedance days were modeled as beta-binomially distributed random variables, which allows for the probability of exceedance on any given day to vary from year to year as a function of annual mean sea level and the amplitude of the highest tides.

We combined the statistical model of exceedance days with predictions of astronomical tides and projections of LMSL to produce probabilistic projections of threshold exceedance days in Honolulu during the 21st century. The inclusion of tidal amplitude as a predictor of future flood frequency elucidates subtleties of future flood frequency not captured by methodologies focused on mean sea level alone (e.g., Vandenberg-Rodes et al., 2016). Specifically, for a threshold of 35 cm above MHHW—the approximate threshold for impacts experienced in Honolulu during 2017—projections of exceedance days per year show a pronounced inflection during the 2030s (section 4.1). After a decade of little change, the expected number of exceedance days per year for the Kopp14 LMSL rise scenario increases fivefold from about 20 in the early 2030s to around 100 by the early 2040s. The pause followed by a rapid increase occurs due to the interaction between increasing rates of LMSL rise and the 18.6-year modulation of tidal amplitude in Honolulu. The modulation of tidal amplitude counters the effect of SLR when tidal amplitude is decreasing and amplifies the effect when tidal amplitude is increasing. Thus, there will be extended periods of time when tidal amplitude is decreasing that the frequency of exceedances above static thresholds will appear to stall even as mean sea level continues to rise. This should not be the basis for inaction, however, as the “tide will turn,” and extended periods of minimal change are likely to be followed by extended periods of rapid increase in threshold exceedances.

The probabilistic projections of exceedance days should be interpreted with consideration of the tendency for events to cluster in time. Planning for the “typical” future year (i.e., the expected or most likely number of exceedance days in a probabilistic sense) can substantially underestimate the number of exceedances during inevitable severe years (section 4.2.1). A prudent approach to planning acknowledges and incorporates the inevitability of severe years rather than focusing on the most likely outcome for a specific year. In support of such an approach, it may be useful to ask when an impactful number of exceedance days will first occur (section 4.2.2) rather than prescribing a specific number of exceedance days with large uncertainty to a future year (section 4.1). The probabilistic nature of the projections developed here allows for complimentary calculations that extract such information. According to the Kopp14 LMSL rise scenario, Honolulu is more likely than not to experience the first year with more than 50 minor flooding days above the 35-cm threshold by 2035 and more than 100 minor flooding days by 2045. Widespread, disruptive impacts above the 90-cm threshold are more likely than not to occur three times or more in a year prior to 2080. We note, however, that the NOAA intermediate-high scenario projects at least three exceedance days above 90 cm in a single year at some point prior to the mid-2050s.

Results demonstrate how quickly exceedance days above a threshold in Honolulu will transition from occasional to chronic (section 4.2.3). Over the next 1–3 decades depending on LMSL rise scenario, the minor flooding impacts experienced in Honolulu on 15 days during 2017 will likely become a chronic circumstance, occurring on at least 50 days in 9 out of 10 years and at least 100 days in 6 out of 10 years. Such transitions will occur even faster at higher thresholds as the rate of LMSL rise increases during the 21st century. Thus, depending on the severity and spatial extent of impacts associated with exceedances above a given threshold, the financial and infrastructural requirements for adaptation and mitigation may require plans to be developed and enacted long before exceedances become even occasional events. A wait-and-see approach

may be insufficient, especially later in the century when the transition from occasional to chronic can occur in less than a decade due to the potential for rates of LMSL rise three times (or more) faster than present.

Finally, we stress that the thresholds utilized in this analysis are subjectively chosen, and the threshold associated with minor flooding (or any impact level) is a function of space and time. No single threshold can adequately summarize present and future impacts across an entire city or region. The level that constitutes minor impacts in one area may be devastating or benign in another. Every incremental change in LMSL will bring minor flooding to new areas and increase the disruptiveness of events in areas already affected. Thus, locally relevant thresholds are essential for accurate impact assessments.

Acknowledgments

The authors thank Matthew M. Barbee of SOEST, University of Hawai'i at Mānoa for providing the digital elevation map of Oahu modified to include the effect of groundwater on inundation. The authors also thank Christopher G. Piecuch of Woods Hole Oceanographic Institution for helpful perspectives on a preliminary version of the manuscript. Authors Thompson and Becker acknowledge support from the United States Geological Survey via the Pacific Islands Climate Adaptation Science Center (Grant No. G15AP00140). Authors Widlansky and Merrifield acknowledge support from the NOAA Modeling, Analysis, Predictions and Projections (MAPP) program (Grant No. NA17OAR4310110). Direct links to all data sources can be found in the text.

References

- Buchanan, M. K., Oppenheimer, M., & Kopp, R. E. (2017). Amplification of flood frequencies with local sea level rise and emerging flood regimes. *Environmental Research Letters*, *12*(6), 64009. <https://doi.org/10.1088/1748-9326/aa6cb3>
- Caldwell, P. C., Merrifield, M. A., & Thompson, P. R. (2010). Sea level measured by tide gauges from global oceans as part of the Joint Archive for Sea Level (JASL) since 1846. <https://doi.org/10.7289/V5V40S7W>
- Chavanne, C., Flament, P., Lumpkin, R., Dousset, B., & Bentamy, A. (2002). Scatterometer observations of wind variations induced by oceanic islands: Implications for wind-driven ocean circulation. *Canadian Journal of Remote Sensing*, *28*(3), 466–474. <https://doi.org/10.5589/m02-047>
- Church, J. A., Clark, P. U., Cazenave, A., Gregory, J. M., Jevrejeva, S., Levermann, A., et al. (2013). Sea Level Change. In T. F. Stocker, D. Qin, G.-K. Plattner, et al. (Eds.), *Climate change 2013: The physical science basis. Contribution of working group I to the fifth assessment report of the intergovernmental panel on climate change* (pp. 1137–1216). Cambridge, United Kingdom and New York, NY, USA: Cambridge University Press.
- Cid, A., Menéndez, M., Castanedo, S., Abascal, A. J., Méndez, F. J., & Medina, R. (2016). Long-term changes in the frequency, intensity and duration of extreme storm surge events in southern Europe. *Climate Dynamics*, *46*(5-6), 1503–1516. <https://doi.org/10.1007/s00382-015-2659-1>
- Codiga, D. L. (2011). Unified tidal analysis and prediction using the UTide Matlab functions (*Technical Report 2011-01, (Tech. Rep.)*): Narragansett, RI: Graduate School of Oceanography, University of Rhode Island.
- Cubasch, U., Wuebbles, D., Chen, D., Facchini, M. C., Frame, D., Mahowald, N., & Winther, J.-G. (2013). Introduction. In T. F. Stocker, D. Qin, G.-K. Plattner, et al. (Eds.), *Climate change 2013: The physical science basis. contribution of working group I to the fifth assessment report of the intergovernmental panel on climate change* (pp. 119–158). Cambridge, United Kingdom and New York, NY, USA: Cambridge University Press.
- Dahl, K. A., Fitzpatrick, M. F., & Spanger-Siegfried, E. (2017). Sea level rise drives increased tidal flooding frequency at tide gauges along the U.S. East and Gulf Coasts: Projections for 2030 and 2045. *PLOS ONE*, *12*(2), e0170949. <https://doi.org/10.1371/journal.pone.0170949>
- Firing, Y. L., & Merrifield, M. A. (2004). Extreme sea level events at Hawaii: Influence of mesoscale eddies. *Geophysical Research Letters*, *31*, L24306. <https://doi.org/10.1029/2004GL021539>
- Firing, Y. L., Merrifield, M. A., Schroeder, T. A., & Qiu, B. (2004). Interdecadal sea level fluctuations at Hawaii. *Journal of Physical Oceanography*, *34*(11), 2514–2524. <https://doi.org/10.1175/JPO2636.1>
- Habel, S., Fletcher, C. H., Rotzoll, K., & El-Kadi, A. I. (2017). Development of a model to simulate groundwater inundation induced by sea-level rise and high tides in Honolulu, Hawaii. *Water Research*, *114*, 122–134. <https://doi.org/10.1016/j.watres.2017.02.035>
- Haigh, I. D., Eliot, M., & Pattiaratchi, C. (2011). Global influences of the 18.61 year nodal cycle and 8.85 year cycle of lunar perigee on high tidal levels. *Journal of Geophysical Research*, *116*, C06025. <https://doi.org/10.1029/2010JC006645>
- Hall, J. A. J., Gill, S., Obeysekera, J., Sweet, W., Knuuti, K., & Marburger, J. (2016). Regional sea level scenarios for coastal risk management: managing the uncertainty of future sea level change and extreme water levels for Department of Defense coastal sites worldwide (*Tech. Rep.*) Alexandria, Virginia: U.S. Department of Defense, Strategic Environmental Research and Development Program.
- Hawai'i Climate Change Mitigation and Adaptation Commission (2017). Hawai'i sea level rise vulnerability and adaptation report (*Tech. Rep.*) Department of Defense, Strategic Environmental Research and Development Program. <https://doi.org/10.13140/RG.2.2.31307.39208>
- Kim, J., & Lee, J.-H. (2017). The validation of a beta-binomial model for overdispersed binomial data. *Communications in Statistics - Simulation and Computation*, *46*(2), 807–814. <https://doi.org/10.1080/03610918.2014.960091>
- Kopp, R. E., Horton, R. M., Little, C. M., Mitrovica, J. X., Oppenheimer, M., Rasmussen, D. J., et al. (2014). Probabilistic 21st and 22nd century sea-level projections at a global network of tide-gauge sites. *Earth's Future*, *2*(8), 383–406. <https://doi.org/10.1002/2014EF000239>
- LaFrance, A. (2017). The ghost of climate-change future. Retrieved from <https://www.theatlantic.com/science/archive/2017/05/the-ghost-of-climate-change-future/528471/>
- Marcos, M., Calafat, F. M., Berihuete, Á., & Dangendorf, S. (2015). Long-term variations in global sea level extremes. *Journal of Geophysical Research: Oceans*, *120*, 8115–8134. <https://doi.org/10.1002/2015JC011173>
- Moftakhari, H. R., AghaKouchak, A., Sanders, B. F., & Matthew, R. A. (2017). Cumulative hazard: The case of nuisance flooding. *Earth's Future*, *5*(2), 214–223. <https://doi.org/10.1002/2016EF000494>
- OCM Partners (2018). 2013 USACE NCMP Topobathy Lidar: Oahu (HI) - LMSL. NOAA National Centers for Environmental Information. Retrieved from <https://inport.nmfs.noaa.gov/inport/item/49755>
- Olsen, J., Rolf, Lambert, J. H., & Haines, Y. Y. (1998). Risk of extreme events under nonstationary conditions. *Risk Analysis*, *18*(4), 497–510. <https://doi.org/10.1111/j.1539-6924.1998.tb00364.x>
- Pickering, M. D., Horsburgh, K. J., Blundell, J. R., Hirschi, J. J.-M., Nicholls, R. J., Verlaan, M., & Wells, N. C. (2017). The impact of future sea-level rise on the global tides. *Continental Shelf Research*, *142*(September 2016), 50–68. <https://doi.org/10.1016/j.csr.2017.02.004>
- Rasmussen, DJ, Bittermann, K., Buchanan, M. K., Kulp, S., Strauss, B. H., Kopp, R. E., & Oppenheimer, M. (2018). Extreme sea level implications of 1.5 ° C, 2.0 ° C, and 2.5 ° C temperature stabilization targets in the 21st and 22nd centuries. *Environmental Research Letters*, *13*(3), 34040. <https://doi.org/10.1088/1748-9326/aaac87>
- Ray, R. D., & Foster, G. (2016). Future nuisance flooding at Boston caused by astronomical tides alone. *Earth's Future*, *4*(12), 578–587. <https://doi.org/10.1002/2016EF000423>

- Skellam, JG (1948). A probability distribution derived from the binomial distribution by regarding the probability of success as variable between the sets of trials. *Journal of the Royal Statistical Society. Series B (Methodological)*, 10(2), 257–261.
- Sweet, W. V., Dusek, G., Obeysekera, J., & Marra, J. J. (2018). Patterns and projections Of high tide flooding along the U.S. coastline using a common impact threshold (NOAA Technical Report NOS CO-OPS 086). Silver Spring, Maryland: U.S. Department of Commerce, National Oceanic and Atmospheric Administration, National Ocean Service Center for Operational Oceanographic Products and Services.
- Sweet, W. V., Kopp, R. E., Weaver, C. P., Obeysekera, J., Horton, R. M., Thieler, E. Robert, & Zervas, C. (2017). Global and regional sea level rise scenarios for the United States (NOAA Technical Report NOS CO-OPS 083). Silver Spring, Maryland: U.S. Department of Commerce, National Oceanic and Atmospheric Administration, National Ocean Service Center for Operational Oceanographic Products and Services.
- Sweet, W. V., Park, J., Marra, J. J., Zervas, C., & Gill, S. (2014). Sea level rise and nuisance flood frequency changes across the United States (NOAA Technical Report NOS CO-OPS 073). Silver Spring, Maryland: U. S. Department of Commerce, NOAA, NOS Center for Operational Oceanographic Products and Services.
- Tebaldi, C., Strauss, B. H., & Zervas, C. E. (2012). Modelling sea level rise impacts on storm surges along US coasts. *Environmental Research Letters*, 7(1), 14032. <https://doi.org/10.1088/1748-9326/7/1/014032>
- University of Hawai'i Sea Grant College Program (2016). Hawai'i and Pacific Islands King Tides Project. Retrieved from <http://seagrant.soest.hawaii.edu/coastal-and-climate-science-and-resilience/ccs-projects/hawaii-pacific-islands-king-tides-project/>
- Vandenberg-Rodes, A., Moftakhari, H. R., AghaKouchak, A., Shahbaba, B., Sanders, B. F., & Matthew, R. A. (2016). Projecting nuisance flooding in a warming climate using generalized linear models and Gaussian processes. *Journal of Geophysical Research: Oceans*, 121, 8008–8020. <https://doi.org/10.1002/2016JC012084>
- Wahl, T., Haigh, ID, Nicholls, RJ, Arns, A., Dangendorf, S., Hinkel, J., & Slangen, ABA (2017). Understanding extreme sea levels for broad-scale coastal impact and adaptation analysis. *Nature Communications*, 8, 16075. <https://doi.org/10.1038/ncomms16075>
- Wdowinski, S., Bray, R., Kirtman, B. P., & Wu, Z. (2016). Increasing flooding hazard in coastal communities due to rising sea level: Case study of Miami Beach, Florida. *Ocean & Coastal Management*, 126, 1–8. <https://doi.org/10.1016/j.ocecoaman.2016.03.002>
- Widlansky, M. J., Marra, J. J., Chowdhury, R. Md., Stephens, S. A., Miles, E. R., Fauchereau, N., et al. (2017). Multimodel ensemble sea level forecasts for tropical Pacific islands. *Journal of Applied Meteorology and Climatology*, 56(4), 849–862. <https://doi.org/10.1175/JAMC-D-16-0284.1>
- Widlansky, M. J., Timmermann, A., & Cai, W. (2015). Future extreme sea level seesaws in the tropical Pacific. *Science Advances*, 1(8), e1500560. <https://doi.org/10.1126/sciadv.1500560>
- Yoon, H., Widlansky, M. J., & Thompson, P. R. (2018). Nu'a Kai: Flooding in Hawaii caused by a “stack” of oceanographic processes [in State of the Climate in 2017]. *Bulletin of the American Meteorological Society*, 99(8), S88–S89. <https://doi.org/10.1175/2018BAMSStateoftheClimate.1>

References from Supporting Information

- Duane, S., Kennedy, A. D., Pendleton, B. J., & Roweth, D. (1987). Hybrid Monte Carlo. *Physics Letters B*, 195(2), 216–222. [https://doi.org/10.1016/0370-2693\(87\)91197-X](https://doi.org/10.1016/0370-2693(87)91197-X)
- Gelman, A., Carlin, J. B., Stern, H. S., Dunson, D. B., Vehtari, A., & Rubin, D. B. (2013). Bayesian data analysis (pp. 1–639).
- Hoffman, M. D., & Gelman, A. (2014). The No-U-Turn Sampler: Adaptively setting path lengths in Hamiltonian Monte Carlo. *Journal of Machine Learning Research*, 15(1), 1593–1623.
- Salvatier, J., Wiecki, T. V., & Fonnesbeck, C. (2016). Probabilistic programming in Python using PyMC3. *PeerJ Computer Science*, 2, e55. <https://doi.org/10.7717/peerj-cs.55>